Published in final edited form as:
Bioconjug Chem. 2012 February 15; 23(2): 184–195. doi:10.1021/bc200436x.

Fibronectin Binding to the *Treponema pallidum* Adhesin Protein Fragment rTp0483 on Functionalized Self-Assembled Monolayers

Matthew T. Dickerson[a], **Morgan B. Abney**[a], **Caroline E. Cameron**[b], **Marc Knecht**[c], **Leonidas G. Bachas**[c], and **Kimberly W. Anderson**[a,*]

[a]Chemical and Materials Engineering, University of Kentucky, Lexington, KY 40506-0054, USA

[b]Department of Biochemistry and Microbiology, University of Victoria, Victoria, BC V8P 5C2, Canada

[c]Department of Chemistry, University of Miami, Miami, FL, 33124-4620, USA

Abstract

Past work has shown that *Treponema pallidum*, the causative agent of syphilis, binds host fibronectin (FN). FN and other host proteins are believed to bind to rare outer membrane proteins (OMPs) of *T. pallidum*, and it is postulated that this interaction may facilitate cell attachment and mask antigenic targets on the surface. This research seeks to prepare a surface capable of mimicking the FN binding ability of *T. pallidum* in order to investigate the impact of FN binding with adsorbed Tp0483 on the host response to the surface. By understanding this interaction it may be possible to develop more effective treatments for infection and possibly mimic the stealth properties of the bacteria. Functionalized self-assembled monolayers (SAMs) on0 gold were used to investigate rTp0483 and FN adsorption. Using a quartz crystal microbalance (QCM) rTp0483 adsorption and subsequent FN adsorption onto rTp0483 was determined to be higher on negatively charged carboxylate-terminated self-assembled monolayers ($-COO^-$ SAMs) compared to the other surfaces analyzed. Kinetic analysis of rTp0483 adsorption using surface plasmon resonance (SPR) supported this finding. Kinetic analysis of FN adsorption using SPR revealed a multi-step event, where the concentration of immobilized rTp0483 plays a role in FN binding. An examination of relative QCM dissipation energy compared to the shift in frequency showed a correlation between the physical properties of adsorbed rTp0483 and SAM surface chemistry. In addition, AFM images of rTp0483 on selected SAMs illustrated a preference of rTp0483 to bind as aggregates. Adsorption on $-COO^-$ SAMs was more uniform across the surface, which may help further explain why FN bound more strongly. rTp0483 antibody studies suggested the involvement of amino acids 274–289 and 316–333 in binding between rTp0483 to FN, while a peptide blocking study only showed inhibition of binding with amino acids 316–333. Finally, surface adsorbed rTp0483 with FN bound significantly less anti-RGD and gelatin compared to FN adsorbed directly to $-COO^-$ SAMs indicating that one or both binding regions may play a role in binding between rTp0483 and FN.

Keywords

Self assembly; Fibronectin; Protein adsorption; Antigenic disguise

*Corresponding author: Department of Chemical and Materials Engineering, University of Kentucky, 177 F. Paul Anderson Tower, Lexington, KY 40506-0046, USA. Tel.: + 1 859 257 4815; fax: 859 323 1929. kanderson@engr.uky.edu.

SUPPORTING INFORMATION

Figures noted in the text. This material is available free of charge via the Internet at http://pubs.acs.org.

INTRODUCTION

Syphilis is a chronic, multi-stage disease caused by the spirochete bacterium *Treponema pallidum.* The scarcity of antigenic targets on the surface of the bacterium is thought to play a role in the ability of *T. pallidum* to evade the immune response and establish a chronic infection.[1–9] *T. pallidum* elicits an acute immune response during 0the primary stage of the disease, after which the disease enters a latent phase that is characterized by periodic reoccurrence of disease symptoms. The primary factor responsible for the capacity of *T. pallidum* to establish prolonged periods of latency is believed to be the unique composition of the *T. pallidum* outer membrane. The surface of *T. pallidum* lacks lipopolysaccharide, which is a potent modulator of inflammation, and displays a dearth of surface proteins.[5, 10] The initial immune response is likely due to recognition of one or more antigenic outer membrane proteins OMPs on the bacterium, but it remains unclear why a portion of the bacteria are able to persist within the host and produce a secondary infection at a later time.[1, 4, 6–9]

Studies have shown that *T. pallidum* binds to a number of extracellular matrix (ECM) components, including fibronectin (FN), as a method of adherence and infiltration through the host.[1–3, 11–13] FN is a common protein found in the blood as well as in the ECM. A number of proteins of the integrin family as well as a number of other biologically important molecules like fibrin, collagen, and heparin are known to interact with FN.[14] One possible explanation for the propensity of *T. pallidum* to circumvent the detrimental effects of antibodies and immune effector cells is that host proteins, such as fibronectin, become bound to exposed antigenic targets and render them inaccessible to host defense mechanisms. In a study by Cameron *et al.* two putative outer membrane proteins of *T. pallidum* capable of binding FN, identified as Tp0483 and Tp0155, were expressed as recombinant protein fragments.[3] The C-terminal fragment of Tp0483 employed in the study was shown to retain expected FN binding capacity. In addition, work by Brinkman *et al.* identified a third putative membrane protein (Tp0136) that demonstrated similar affinity for the ECM components FN and laminin.[1] While Tp0483, Tp0155, and Tp0136 all bound insoluble ECM FN, only Tp0483 showed an affinity for soluble FN.[3] Binding of ECM FN can be reasonably assumed to be for the purpose of host attachment and tissue infiltration; however, the pathogenic advantage conferred by soluble FN binding to the bacterium remains unclear. Here, it is postulated that soluble FN is bound for the purpose of obscuring exposed antigenic targets from detection. This property is referred to as antigenic disguise.

This work seeks to better characterize the hypothesized interaction between Tp0483 and FN as well as prepare a surface capable of mimicking the FN binding properties of *T. pallidum*. Such a coating could possibly mimic the antigenic disguise properties of whole *T. pallidum* and lead to a reduction in adverse reactions to synthetic materials in the body. Tp0483 was selected because of its ability to bind soluble FN. The recombinant C-terminal portion of Tp0483 (rTp0483) expressed in Cameron *et al.* was examined to determine its ability to bind soluble FN on a range of surface chemistries in an attempt to mimic the interaction between FN and natural Tp0483 found on the surface of *T. pallidum.*[3] Physical adsorption of rTp0483 on self-assembled monolayers (SAMs) and subsequent FN adsorption to rTp0483 were investigated using quartz crystal microbalance (QCM) and surface plasmon resonance spectroscopy (SPR) approaches. Atomic force microscopy (AFM) was used to analyze further the binding of rTp0483 to each of the functionalized SAM surfaces. Two regions of the Tp0483 protein sequence contained within the expressed rTp0483 fragment were identified as probable FN binding sites, following which peptides and antibodies matching these regions were produced to test their involvement in FN binding. Numerous studies have suggested that the RGD cell-binding sequence located in the 10th type III domain of FN

plays a significant role in *T. pallidum* adhesion.[12, 15–17] In addition, a number of other binding domains exist on FN including binding sites specific for heparin and collagen/gelatin.[14] Previous studies have revealed that the binding of certain species of bacteria are modulated by these heparin or collagen/gelatin-binding domains of FN.[18, 19] In order to elucidate a more complete profile of rTp0483 FN binding, anti-RGD, heparin, and gelatin binding were studied to determine their involvement in the binding of FN on surfaces coated with rTp0483 compared to unmodified $-COO^-$ SAMs.

EXPERIMENTAL PROCEDURES

Proteins and Antibodies

Human plasma fibronectin (FN) and all other chemicals not specifically mentioned were purchased from Sigma Aldrich (St. Louis, MO). An antibody against the RGD (Arginine-Glycine-Aspartate) cell-binding site of FN was purchased from Chemicon International (Temecula, TN) and later from Abcam (Cambridge, MA). The protein fragment rTp0483 was expressed and purified based on the procedure used in Cameron *et al.*[20] BL21 (DE3)pLysS cells from Invitrogen (Carlsbad, CA) were transformed with a pRSETc plasmid containing the rTp0483 gene with a 6xHis tag. Protein expression was induced during log-phase growth with 0.5mM isopropyl β-D-thiogalactopyranoside for 3 hours at 30°C, and the cells were recovered by centrifugation at 4,000 RPM for 15 min then lysed with a series of sonication cycles. The pellet was resuspended and sonicated in binding buffer (20 mM Tris, 5 mM imidazole, 0.5 M NaCl, pH 7.9) with 0.1% NP-40 and 1% (v/v) EDTA free, Halt protease inhibitor cocktail (HPIC) Thermo Scientific (Rockford, IL). The lysed cell contents were recovered by centrifugation at 13,000 RPM for 15 min. The pellet was resuspended in binding buffer with 1% (v/v) HPIC, sonicated, and recovered by centrifugation two additional times. Insoluble rTp0483 in the pellet was recovered by suspension in binding buffer with 6 M urea, after which the suspension was applied to a Ni-NTA superflow column from Qiagen (Hilden, Germany). The column was washed with binding buffer also with 6 M urea and 20 mM imidazole. Bound rTp0483 was recovered with elution buffer (20 mM Tris, 0.5 M NaCl, 1 M imidazole, pH 7.9). A process for protein renaturation was adapted from Zhang *et al.*[21] Zwittergent 3–12 was added to the protein to a final concentration of 0.5% (w/v), and the sample was dialyzed consecutively with renaturation buffer 1 (100 mM Tris, 200 mM NaCl, 10 mM EDTA, pH 8.0) and renaturation buffer 2 (50 mM Tris, 200 mM NaCl, 0.5 mM EDTA). The presence of rTp0483 was confirmed with SDS-PAGE and Western Blot (see supporting documentation).

Aves Labs (Tigard, OR) identified two probable FN binding peptide sequences on rTp0483 using Hopp-Woods and Kyte-Doolittle (hydrophilicity), Emini (surface probability), Karplus-Shulz (chain flexibility), and Jameson-Wolf (a combination of attributes) methods. Peptides corresponding to residues 274–289 (D1- QMHSDSKQVDVKLDGN) and 316–333 (D2- QRKEDDSMYSYVTGTMKY) of the complete Tp0483 sequence were prepared along with monoclonal antibodies (anti-Tp0483#1 IgY, chicken # 5507–5508 - against residues 274–289 and anti-Tp0483#2 IgY, chicken # 5509–5510 - against residues 316–333) by Aves Labs. Two other peptides (A3 - AYSSGAPPMPPF and P1 - HSSYWYAFNNKT) were provided for use as negative controls.

Self-Assembled Monolayers (SAMs)

SAMs were assembled on gold QCM and SPR surfaces by incubation overnight in selected 1 mM alkanethiol solutions; 11-mercapto-undecanoic acid was purchased from Sigma Aldrich (St. Louis, MO); 11-hydroxy-1-undecanethiol, 1-dodecanethiol, and 11- amino-1-undecanethiol hydrochloride were purchased from Asemblon (Redmond, WA). Gold QCM surfaces were purchased from Biolin Scientific (Linthicum, MD), and gold SPR surfaces

were purchased from Biacore AB (Uppsala, Sweden). Monolayers were characterized using contact angle analysis and X-ray photoelectron spectroscopy (XPS), and compared to literature values.[22–28] Contact angle studies were completed on a Future Digital Scientific Contact Angle Goniometer (Long Island, NY). XPS data were gathered using Mg from a twin anode XR3E2 X-ray source and the CLAM4MCD analyzer from Thermo VG Scientific (Waltham, MA). Prior to protein adsorption studies, the gold surfaces containing SAMs were removed from their alkanethiol solution and washed for 15 s in ACS grade ethanol followed by deionized (using a Millipore milliQ deionizer) water. The surfaces were dried with ultrapure nitrogen gas just before analysis. After use, surfaces were regenerated by either 5 min immersion in a 5:1:1 mixture of deionized water, ammonium hydroxide, and hydrogen peroxide at 75 °C followed by 10 min exposure to UV/ozone or a 20 min exposure to O_2 plasma at a flow rate of 1 standard ft^3/h (SCFH) and a pressure of 700 mTorr in a PDC-002 (230 V) plasma cleaner with Plasmaflo unit from Harrick Plasma (Ithaca, NY) followed by immersion in ACS grade ethanol for at least 14 h.

rTp0483 and FN Adsorption and Kinetic Modeling

A Q-Sense E4 quartz crystal microbalance (QCM) from Biolin Scientific (Linthicum, MD) was used for both rTp0483 and FN adsorption studies. SAMs were prepared as previously described. Dulbecco's Phosphate Buffered Saline (DPBS, 137 mM NaCl, 2.7 mM KCl, 8 mM Na_2HPO_4, 1.5 mM KH_2PO_4, pH 7.4) was employed as a running buffer in the QCM and used to dilute all proteins to the desired concentration for analysis. Changes in signal as a result of protein adsorption were measured as a frequency change (Δf) in hertz (Hz). Changes in dissipation energy (D) were also tracked. Dissipation energy is the sum of all energy lost from the system during a single oscillation divided by the total energy in the system. This parameter is related to the physical properties of an adsorbed layer. Factors such as hydration and layer fluidity can lead to increases in the dissipation energy of a sample and, based on this, it is possible to compare the binding state of proteins on different surfaces. A simple Sauerbrey equation was employed to estimate the surface mass density of adsorbed protein.[29, 30]

$$\Gamma = -\frac{C}{n}\Delta f \tag{1}$$

Here Γ is the surface mass density (pg/mm^2), n is the QCM overtone (n = 1, 3, 5, 7, 9), and C is a constant for a quartz crystal of a specified resonant frequency. Overtone refers to the oscillation frequency of the QCM crystal relative to its fundamental frequency. In this case, the fundamental frequency of the crystal was 5 MHz and C = 177 $pg/Hz{\bullet}mm^2$. So for example, the 3rd overtone corresponds to three times the fundamental frequency or 15 MHz. In order to employ this expression, the adsorbed layer was assumed to be homogeneous and rigid with a no slip condition between the gold layer and adsorbed protein.[29, 30] To fulfill these conditions, dissipation energy of less than 10^{-5} is required.[30] Moreover, when dissipation energy is low, it can be assumed that the deviation between overtones is negligible. For this study, data corresponding to the 9th overtone were used.

To investigate protein adsorption, 20 μg rTp0483/mL was introduced into the system for 2 min at 50 μL/min. Two mg BSA/mL was then introduced for 2 min at 50 μL/min to block the surface not covered by rTp0483 and, hence, prevent nonspecific binding of FN. Finally, 100 μg FN/mL was introduced into the QCM for 2 min at 50 μL/min. Prior to and after the introduction of each protein, surfaces were equilibrated with DPBS at a flow rate of 50 μL/min until the QCM signal stabilized.

A surface plasmon resonance (SPR) spectrometer (Biacore X from Biacore AB (Uppsala, Sweden)) was used for all kinetic studies. SAMs were prepared as previously described.

DPBS was employed as a running buffer and was used to dilute all proteins to the desired concentrations. Any change in SPR signal was measured in response units (RU), where a change of 1 RU was equivalent to a change of 1 pg/mm^2 of protein on the surface.[31]

To investigate the kinetics of rTp0483 binding, 100 μL of rTp0483 was injected at concentrations of 5, 10, and 20 μg rTp0483/mL at 50 μL/min. The corresponding adsorption sensorgrams were analyzed using Biacore BIAevaluation software v3.0.2 to model kinetic parameters.

For FN kinetic analysis, 100 μL of rTp0483 was injected at 5 and 20 μg rTp0483/mL at 50 μL/min. A volume of 100 μL of 2 mg BSA/mL was injected to block the surface not covered by rTp0483 at 50 μL/min. Finally, 100 μL of FN was injected at concentrations of 10, 20, and 40 μg FN/mL at 50 μL/min. These lower FN concentrations were used in order to limit the potential of mass transport effects. The corresponding adsorption sensorgrams were analyzed using Biacore BIAevaluation software v3.0.2 in order to model kinetic parameters. As with the QCM studies, each surface was equilibrated with DPBS at a flow rate of 50 μL/min until the SPR signal stabilized prior to and after each protein injection.

In order to determine the effect of surface chemistry on rTp0483 binding and subsequently FN binding to rTp0483 on the selected SAMs, the kinetics of rTp0483 and FN adsorption were modeled using the Biacore BIAevaluation software v3.0.2 package. Adsorption was compared on the selected SAMs representing negatively charged, positively charged, hydrophilic, and hydrophobic surface chemistries. rTp0483 and FN were adsorbed onto SAM surfaces under the conditions detailed above, and both binding and dissociation kinetics were obtained in order to determine binding affinity. The strength of protein binding was represented by an affinity constant (K_A) for each surface, where K_A was calculated by dividing the rate of protein binding by the rate of protein dissociation. Direct rTp0483 binding to each surface was modeled as a simple 1:1 Langmuir binding event. For comparison, a model including mass transport effects was also generated. FN binding to adsorbed rTp0483 on $-COO^-$ functionalized SAMs was also modeled based on 1:1 Langmuir binding with and without mass transport limitations; however, neither model adequately represented the adsorption event. FN is a dimeric protein so each FN molecule has the potential to bind two molecules of rTp0483. A bivalent model was used in order to represent this aspect of FN. A bivalent model with mass transport limitations was also analyzed (data not shown); however, the fit was poor indicating that for FN adsorption onto rTp0483 there were no mass transport limitations.

1:1 Langmuir Binding—The binding kinetics for 1:1 Langmuir binding are represented in Equation 2 and the related rate equations are summarized in Equations 3 and 4. *A* is rTp0483 or FN, *B* is a binding site on the surface, and *AB* is a protein A bound to site *B* on the surface. The bulk concentration of A was assumed to be constant thus the rate equations were written with respect to the change in the number of occupied sites on the surface.

$$A + B \Longleftrightarrow AB \tag{2}$$

$$\frac{\partial [B]}{\partial t} = -(k_a[A][B] - k_d[AB]) \tag{3}$$

$$\frac{\partial [AB]}{\partial t} = k_a[A][B] - k_d[AB] \tag{4}$$

The injected concentration was known for each test, and the number of occupied sites was assumed to be zero initially ($[AB]_0=0$). The maximum binding capacity (R_{max}) was determined empirically for each surface and assumed to be equal to the number of sites B initially ($[B]_0=R_{max}$). Adsorption sensorgrams at the aforementioned concentrations were generated. The binding and dissociation kinetics were determined using BIAevaluation software v3.0.2 and used to calculate K_A.

1:1 Langmuir Binding with Mass Transport Limitations—In this model, the prior 1:1 model was modified to account for limitations in the transfer of A from bulk solution to the surface. Equations 5 and 6 illustrate the modified process. The impact on binding kinetics was accounted for through the inclusion of an additional term as shown in Equation 7. This term includes a mass transfer coefficient (k_t) along with a term for the bulk concentration of A in solution ($[A]_s$), which was taken be a constant value. The remaining rate equations are shown in Equations 8 and 9.

$$A_s \Longleftrightarrow A \tag{5}$$

$$A+B \Longleftrightarrow AB \tag{6}$$

$$\frac{\partial[A]}{\partial t}=k_t([A]_s-[A])-(k_a[A][B]-k_d[AB]) \tag{7}$$

$$\frac{\partial[B]}{\partial t}=-(k_a[A][B]-k_d[AB]) \tag{8}$$

$$\frac{\partial[AB]}{\partial t}=k_a[A][B]-k_d[AB] \tag{9}$$

As previously discussed, the injected concentration was known, all sites were assumed to empty initially ($[AB]_0=0$), and the total number of sites was determined empirically for each surface that was analyzed ($[B]_0=R_{max}$). Additionally, the concentration of A was assumed to be zero initially ($[A]_0=0$). BIAevaluation software v3.0.2 was used to determine the binding and dissociation kinetics based on adsorption sensorgrams and then used to calculate K_A.

Bivalent Analyte—A bivalent analyte adsorption model represents a system where an analyte (A) binds to a ligand (B) as described above; however, once *AB* is formed, it further reacts with a second ligand *B* resulting in the complex AB_2. In this case A was FN and B was adsorbed rTp0483. Like 1:1 Langmuir binding, the concentration of A was assumed to be constant, and the equations solved with respect to sites on the surface occupied by either AB or AB_2. These reactions are represented below in Equations 10 and 11 and the corresponding rate equations are shown in Equations 12–14.

$$A+B \Longleftrightarrow AB \tag{10}$$

$$AB+B \Longleftrightarrow AB_2 \tag{11}$$

$$\frac{\partial[B]}{\partial t}=-(k_{a1}[A][B]-k_{d1}[AB])-(k_{a2}[AB][B]-k_{d2}[AB_2]) \tag{12}$$

$$\frac{\partial[AB]}{\partial t} = (k_{a1}[A][B] - k_{d1}[AB]) - (k_{a2}[AB][B] - k_{d2}[AB_2]) \quad (13)$$

$$\frac{\partial[AB_2]}{\partial t} = k_{a2}[AB][B] - k_{d2}[AB_2] \quad (14)$$

The same assumptions were made for this model as detailed above. In addition, the initial concentration of AB_2 was assumed to be zero ($[AB_2]_0=0$). BIAevaluation software v3.0.2 was used to determine the binding and dissociation kinetics for both reactions based on adsorption sensorgrams and then used to calculate K_{A1} and K_{A2}.

rTp0483 Monolayer Dissipation Energy Analysis

The Q-Sense E4 was employed for the analysis of rTp0483 monolayer dissipation energy. SAMs were prepared as previously described. For dissipation energy studies, 100 μg rTp0483/mL was injected into the QCM for 2 min at 50 μL/min. The higher concentration of rTp0483 was used in this study to produce a more complete protein monolayer. Prior to and after protein binding, each surface was equilibrated with DPBS at a flow rate of 50 μL/min until the SPR signal stabilized. The change in dissipation energy for each surface was divided by the frequency change in order to calculate the dissipation energy as a function of protein surface mass density.

AFM Imaging of rTp0483 on SAMs

A Molecular Imaging PicoSPM from Agilent Technologies (Tempe, AZ) using Tap300 Intermittent Contact Tips from Budget Tips (Sofia, Bulgaria) was used to provide images of rTp0483 adsorption on each of the SAMs. Data analysis was completed using PicoScan Software (Agilent Technologies) and Gwyddion Software 2.5 (General Public License, development supported by the Czech Metrology Institute, Brno, Czech Republic). Freshly prepared SAMs were incubated in a solution of 10 μg rTp0483/mL for 15 min at room temperature. Surfaces were rinsed with milliQ water, dried with ultrapure nitrogen gas, and imaged immediately.

rTp0483 Binding Domain Analysis

The Biacore X SPR spectrometer was used for all anti-rTp0483 antibody and rTp0483 peptide studies. SAMs were prepared as previously described. The selected rTp0483 antibodies were prepared at a concentration of 200 μg antibody/mL. Initially, 100 μL of 20 μg rTp0483/mL was injected and adsorbed onto a surface at 50 μL/min. After stabilization, 100 μL of 2 mg BSA/mL was injected to block the surface not covered by rTp0483 at 50 μL/min. To test the effect of FN on antibody binding, 100 μL of 100 μg FN/mL was injected at 50 μL/min and, once the SPR signal was stable, 100 μL of anti-Tp0483#1 or anti-Tp0483#2 were injected at 50 μL/min. Nonspecific antibody binding on the BSA blocked portion of the surface was analyzed by injecting 100 μL of 2 mg BSA/mL at 50 μL/min followed by 100 μL of anti-Tp0483#1 or anti-Tp0483#2 at 50 μL/min. Prior to protein binding, each surface was equilibrated with DPBS at a flow rate of 50 μL/min until the SPR signal stabilized.

In order to determine the effect of rTp0483 antibodies on FN binding rTp0483 was injected followed by BSA as detailed previously. This was followed by 100 μL of anti-Tp0483#1 or anti-Tp0483#2 at 50 μL/min. Once the SPR signal was stable, 100 μL of 100 μg FN/mL was injected at 50 μL/min.

Because the analogous rTp0483 antibodies bound to rTp0483 only on negatively charged SAMs, only −COO⁻ terminated SAMs were examined in these studies. Samples containing a 20:1 molar ratio of a specific rTp0483 peptide or a nonspecific control peptide and FN were prepared. First, 100 μL of 20 μg rTp0483/mL was injected and adsorbed to each surface at 50 μL/min. After stabilization, 100 μL of 2 mg BSA/mL was injected to block the surface not covered by rTp0483 at 50 μL/min. After the SPR signal stabilized, 100 μL of one of the 20:1 peptide/FN solutions was injected at 50 μL/min. Alternately, after rTp0483 had been adsorbed and blocked with BSA, 100 μL of 100 μg FN/mL was injected for comparison at 50 μL/min. Prior to and after protein binding, each surface was equilibrated with DPBS at a flow rate of 50 μL/min until the SPR signal stabilized. Binding inhibition was determined using Equation 15:

$$\%\ FN\ binding = \frac{FN{+}peptide\ on\ rTp0483\ \left(\frac{pg}{mm^2}\right)}{FN\ on\ rTp0483\ \left(\frac{pg}{mm^2}\right)} \times 100\% \tag{15}$$

FN Binding Domain Analysis

The Biacore X SPR spectrometer was used for all FN binding domain studies. SAMs were prepared as previously described. Because FN bound preferentially to rTp0483 adsorbed on negatively charged surfaces, only −COO⁻ terminated SAMs were analyzed in these tests. First, 100 μL of 100 μg rTp0483/mL was injected and adsorbed onto a −COO⁻ terminated SAM at 50 μL/min. After the SPR signal stabilized, 100 μL of 100 μg FN/mL was injected at 50 μL/min. The signal was again allowed to stabilize, and then 50 μL of 2 mg heparin/mL was injected at 50 μL/min. Alternately, 100 μL of 100 μg FN/mL was injected and adsorbed onto a −COO⁻ terminated SAM without rTp0483 at 50 μL/min followed by 50 μL of 2 mg/mL heparin at 50 μL/min. This process was repeated for anti-RGD (20 μg/mL) and type A gelatin (1 mg/mL). Prior to and after protein binding, each surface was equilibrated with DPBS at a flow rate of 50 μL/min until the SPR signal stabilized.

As the RGD peptide sequence had previously been implicated in the adhesion of *T. pallidum* to FN, the interaction via this site was further characterized. The Biacore X was used to analyze the involvement of the RGD peptide sequence in the binding of FN to surface-adsorbed rTp0483 on −COO⁻ functionalized SAMs. SAMs were prepared as previously described. A volume of 100 μL of 20 μg rTp0483/mL was injected over the course of 2 min at 50 μL/min. Then, 100 μL of 2 mg BSA/mL was injected to block the surface not covered by rTp0483 at 50 μL/min. After signal stabilization, 50 μL of FN blocked with 20 μg/mL or 50 μg/mL was injected to evaluate adsorption onto rTp0483 over a 1 min period at 50 μL/min. This lower FN concentration was employed in order to minimize the volume of RGD antibody required for testing. Alternately, 50 μL of 10 μg FN/mL was injected alone onto adsorbed rTp0483 at 50 μL/min. Nonspecific antibody adsorption was also measured by injecting 50 μL of anti-RGD alone at 20 μg/mL and 50 μg/mL at 50 μL/min. Prior to and after protein binding, each surface was equilibrated with DPBS at a flow rate of 50 μL/min until the SPR signal stabilized. The mass of adsorbed anti-RGD+FN complex was adjusted to account for the added mass of the bound antibodies. Because FN is dimeric, it was assumed that each FN bound two molecules of anti-RGD. This added mass was accounted for multiplying the observed SPR response by a correction factor as shown in Equations 16 and 17.

$$Correction\ Factor = \frac{FN\ M_W}{FN{+}antibody\ M_W} = \frac{440,000\ Da}{440,000\ Da + (2 \times 150,000\ Da)} = 0.595 \tag{16}$$

$$Fibronectin\ concentration = Observed\ concentration \times 0.595 \quad (17)$$

RESULTS

Self-Assembled Monolayers

Functionalized SAMs displaying $-COO^-$, $-OH$, $-NH_3^+$, and $-CH_3$ groups were prepared as previously described. Contact angle and XPS data (see supporting documentation) were determined and compared with literature values.[22–28] The contact angles corresponded well with literature values, and XPS data relating surface composition indicated SAM formation.

rTp0483 and FN Adsorption and Kinetic Modeling

Adsorption results for rTp0483 onto functionalized SAMs are shown in Figure 1A. Results for $-COO^-$ SAMs indicated an average surface mass density of 782 ± 46 pg/mm^2 while $-OH$, $-NH_3^+$, and $-CH_3$ SAMs were 358 ± 80 pg/mm^2, 453 ± 73 pg/mm^2, and 442 ± 30 pg/mm^2, respectively. ANOVA indicated that adsorption on the $-COO^-$ SAMs was significantly greater than the other three surfaces ($p<0.05$) and that all of the other surfaces were indistinguishable.

The adsorption of FN onto rTp0483 on functionalized SAMs is shown in Figure 1B. As previously mentioned, the portion of each surface not covered by rTp0483 was blocked with BSA, hence, any FN adsorption observed is onto rTp0483. Minimal binding of FN was observed to rTp0483 on the $-OH$ (60 ± 28 pg/mm^2), $-NH_3^+$ (363 ± 82 pg/mm^2), and $-CH_3$ (3.5 ± 3.5 pg/mm^2) surfaces, however, the $-COO^-$ SAMs demonstrated significantly higher binding (1380 ± 200 pg/mm^2, $p<0.05$) than the other three surfaces, which were not significantly different from one another. Because there was significantly more FN binding to rTp0483 adsorbed to $-COO^-$ functionalized SAMs, it was the only surface employed for further study of FN binding to adsorbed rTp0483.

rTp0483 was injected into the Biacore X SPR and adsorbed onto functionalized SAMs over a range of concentrations as previously described and the adsorption sensorgrams used to model the kinetics of rTp0483 adsorption. Adsorption data was fit to a 1:1 Langmuir model as well as a 1:1 Langmuir model with mass transfer limitations. The Chi^2 parameter (mean square of signal noise) was used as a gauge of how well each binding model corresponded to experimental results. The lower the Chi^2 value, the more closely a model correlated to the experimental data. In general, Chi^2 should be of the same magnitude as the noise inherent in a fit to be considered acceptable.[32] The best fit was chosen based on the lowest Chi^2 value and, after being chosen, the Chi^2 value was compared to the range of noise in the model versus the experimental data. A 1:1 Langmuir binding model with mass transfer limitations produced the best fit for rTp0483 adsorption. Chi^2 values ranged from 2.5–4.7 RU, while noise deviated from 0 RU up to 10 RU compared to experimental data. Model rTp0483 adsorption and experimental results for each of the selected functionalized SAMs are shown in Figure 2, and the corresponding values for K_A are included in Table 1. The K_A for rTp0483 adsorption to functionalized SAMs was found to be (13.10 ± 0.19) × 10^7 1/M for $-COO^-$ SAMs, (7.23 ± 0.21) × 10^7 1/M for $-OH$ SAMs, (5.12 ± 0.25) × 10^7 1/M for $-NH_3^+$ SAMs, and (4.93 ± 0.08) × 10^7 1/M for $-CH_3$ SAMs. ANOVA analysis indicated significant differences between these values ($p<0.05$) except for $-NH_3^+$ and $-CH_3$ SAMs, which were the same.

Using the Biacore X SPR rTp0483 was injected and adsorbed onto $-COO^-$ SAMs followed by BSA in order to block any uncoated area against nonspecific adsorption. This was followed by the injection and adsorption of FN at a range of concentrations detailed

previously. The resulting adsorption sensorgrams were employed to model the kinetics of FN adsorption onto rTp0483. A bivalent analyte model was found to fit best the adsorption behavior of FN onto rTp0483 immobilized on $-COO^-$ SAMs. Chi^2 values for the bivalent analyte model were 4.0 RU and 4.8 RU for the concentrations of rTp0483 studied, while noise deviated from 0 RU up to 15 RU compared to experimental data. The experimental results of FN adsorption onto rTp0483 immobilized on $-COO^-$ surfaces along with the model fit are shown in Figure 3. The corresponding values for K_{A1} and K_{A2} are included in Table 2. The K_{A1} was found to be slightly higher with 5 μg rTp0483/mL adsorbed to the surface ($(1.53 \pm 0.13) \times 10^9$ 1/M) compared to the value with 20 μg rTp0483/mL adsorbed to the surface ($(1.03 \pm 0.08) \times 10^9$ 1/M). However, the K_{A2} for FN adsorption to rTp0483 was higher when 20 μg rTp0483/mL was adsorbed to the surface ($(4.03 \pm 0.47) \times 10^{-2}$ 1/RU) compared to the value when 5 μg rTp0483/mL was adsorbed ($(2.25 \pm 0.21) \times 10^{-2}$ 1/RU). The second reaction was expressed as a function of surface mass density rather than concentration because it is purely a surface reaction. The dissociation constants (K_{D1}) were calculated by taking the inverse of the first K_A value at each concentration; for 5 μg rTp0483/mL the K_{D1} was 0.65 ± 0.05 nM and for 20 μg rTp0483/mL the K_{D1} was 0.97 ± 0.07 nM, both of which indicate very strong interactions between rTp0483 and FN.

Adsorbed rTp0483 Dissipation Energy Analysis

The changes in dissipation energy divided by the frequency shift for adsorbed rTp0483 are shown in Figure 4. SAM terminal groups were found to have a measureable effect on the relative dissipation energy. Adsorption of rTp0483 on −OH SAMs produced the largest value ($(0.220 \pm 0.013) \times 10^{-6}$ Hz^{-1}) while adsorption of rTp0483 on $-CH_3$ SAMs produced the lowest value ($(0.105 \pm 0.011) \times 10^{-6}$ Hz^{-1}). The values for $-COO^-$ ($(0.1432 \pm 0.0085) \times 10^{-6}$ Hz^{-1}) and $-NH_3^+$ ($(0.1675 \pm 0.0035) \times 10^{-6}$ Hz^{-1}) were located between the two. ANOVA analysis indicated that the ratio of dissipation energy to frequency change for −OH SAMs was higher than the other three groups ($p<0.05$), that the value for $-CH_3$ SAMs was lower than the other three groups ($p<0.05$), and that the values for $-COO^-$ and $-NH_3^+$ SAMs were statistically equivalent.

AFM Imaging of Tp0483 on SAMs

AFM was employed to investigate the surface arrangement of rTp0483 on functionalized SAMs. Figure 5 shows representative AFM images of rTp0483 binding on each of the functionalized SAM layers and compares them to an unfunctionalized gold surface and to a model SAM ($-CH_3$). Based on its molecular weight the average area occupied by a rTp0483 molecule would be expected to be considerably less than the area occupied by the observed protein aggregates. Aggregation was less pronounced on the $-COO^-$ SAM, where the protein was more evenly spread across the entire area. Also, the size of rTp0483 aggregates appeared larger on the $-NH_3^+$ SAM than the other three.

rTp0483 Binding Site Analysis

SPR was used to probe two potential FN binding sites located on rTp0483. Polyclonal antibodies were raised against two amino acid sequences of rTp0483, which were predicted to be surface-exposed and used to determine if they play a role in FN binding to rTp0483. Antibody binding onto rTp0483 adsorbed on $-CH_3$, −OH, and $-NH_3^+$ SAMs was indistinguishable from binding to the respective SAMs in the absence of protein indicating that the targets were inaccessible when bound on these surfaces (results not shown). When considering the $-COO^-$ SAM, significantly more of both antibodies bound to the adsorbed rTp0483 than directly to the unmodified surface ($p<0.05$).

Figure 6A shows that when adsorbed onto rTp0483, FN significantly decreased the binding of both antibodies ($p<0.05$). The binding of anti-Tp0483#1 decreased from 540 ± 28 pg/

mm^2 to 341 ± 19 pg/mm^2, and anti-Tp0483#2 decreased from 465 ± 49 pg/mm^2 to 204 ± 16 pg/mm^2.

Figure 6B shows that when adsorbed rTp0483 on the $-COO^-$ surface was blocked with anti-Tp0483#1 or anti-Tp0483#2, FN adsorption was significantly reduced ($p<0.05$). FN originally bound to rTp0483 at 846 ± 40 pg/mm^2, which decreased to 373 ± 71 pg/mm^2 in the presence of anti-Tp0483#1 and to 270 ± 73 pg/mm^2 in the presence of anti-Tp0483#2.

Figure 6C shows the results of blocking of FN with the peptide sequences corresponding to the selected antibodies. Binding of FN blocked with D1 was indistinguishable from FN alone (92% ± 10%). D2 was shown to have a measurable effect on FN binding, reducing FN binding to 88.0% ± 4.5% of FN alone ($p<0.05$). No inhibition of FN binding was observed for either negative control (A3- 101.9% ± 7.7% and P1- 110% ± 12%).

FN Binding Domain Analysis

Figure 7 shows a comparison of binding of selected molecules to adsorbed FN or rTp0483+FN on $-COO^-$ SAMs. The difference in heparin binding was not statistically significant on FN (61.3 ± 7.0 pg/mm^2) and rTp0483+FN (25 ± 13 pg/mm^2). Binding of anti-RGD antibody on FN (540 ± 72 pg/mm^2) was significantly higher than rTp0483+FN (267 ± 46 pg/mm^2) ($p<0.05$). Binding of gelatin on FN (940 ± 120 pg/mm^2) was significantly greater than on rTp0483+FN (211 ± 12 pg/mm^2) ($p<0.05$).

Figure 8 shows the binding of FN that had been preincubated with anti-RGD and alone to rTp0483 on $-COO^-$ SAMs. The surface mass density bound was 91 ± 25 and 47 ± 33 pg/mm^2 for FN with 20 μg/mL and 50 μg/mL anti-RGD, respectively. The amount of FN alone that bound was 282 ± 15 pg/mm^2. ANOVA indicated that when blocked with anti-RGD at either ratio, FN binding was significantly reduced ($p<0.05$) suggesting the involvement of the RGD peptide sequence in rTp0483 binding. The same test indicated that the difference in binding between the two blocking concentrations was negligible.

DISCUSSION

This work sets out to investigate the interactions between the recombinant protein fragment rTp0483 and human plasma FN on functionalized SAMs displaying a variety of surface chemistries with the goal of further understanding the interactions in order to mimic the FN binding capacity of *T. pallidum*. The long-term goal is to reproduce the ability of *T. pallidum* to interact with host proteins like FN with potential applications in biomaterial development or disease treatment. With this goal in mind, functionalized SAMs were selected because of their versatility in biocompatibility characterization and the attractiveness of their uniform surface chemistry, stability, and ease of synthesis. Such surfaces are widely employed to analyze important factors in biocompatibility such as plasma protein binding, platelet binding and activation, and various complement and coagulation activation processes.[33–37] For this reason, physical protein adsorption onto functionalized SAMs was employed to probe the binding of FN and rTp0483.

QCM analysis indicated that all selected functionalized SAMs bound equal quantities of rTp0483 with the exception of $-COO^-$, which bound significantly more than the other groups as seen in Figure 1A. Likewise, Figure 1B shows that adsorbed rTp0483 on $-COO^-$ SAMs bound significantly more FN than the others under the selected conditions. The rTp0483 kinetic data shown in Table 1 indicated the affinity of rTp0483 for $-COO^-$ SAMs was significantly higher than the other functionalized surfaces. Interestingly, under the conditions employed in the adsorption studies, rTp0483 binding on $-OH$, $-NH_3^+$, and

$-CH_3$ SAMs was similar; however, a kinetic analysis revealed that the K_A was slightly higher on −OH SAMs than the other two.

The apparent similarity in SPR rTp0483 binding data was primarily due to mass transport effects. When mass transport plays a significant role in an adsorption event the process is broken down into two steps. First, the analyte moves from bulk solution to the surface and second the analyte binds to the surface. When mass transport is slower than binding, adsorption is limited by how quickly analyte is transported to the surface, which is the case for rTp0483 adsorption measured by SPR. The rate of mass transport can be increased above the rate of adsorption or the rate of adsorption can be decreased below the rate of mass transport to reduce or eliminate these effects. Decreasing analyte concentration or increasing the number of surface binding sites can accomplish this goal. The sensor area of a QCM substrate is substantially larger than the sensor area of an SPR substrate (154 mm^2 and 1.2 mm^2 respectively), thus by moving from SPR to QCM analysis the number of rTp0483 binding sites was greatly increased while rTp0483 concentration, injection volume, and flow rate remained unchanged. Increase in the rate of mass transport for QCM testing as a result of additional binding sites eliminated mass transport effects and allowed for a more accurate representation of binding kinetics. These results suggest that $-COO^-$ functionalized SAMs provide the best conditions for rTp0483 binding, which is likely due to the high isoelectric point (pI) of the protein. The pI of rTp0483 is 9.3 and since all studies were conducted at a physiological pH (7.4), the protein would possess a net positive charge. This in turn should lead rTp0483 to interact most strongly with the negatively charged SAM via electrostatic interactions.

This idea can also be seen in the dissipation energy data shown in Figure 4. Dissipation energy is a measure of the total energy lost per cycle during QCM operation.[29, 30] The amount of energy lost is related to the physical properties of the material adsorbed on the quartz sensing crystal. A soft, fluid layer deforms while oscillating, which leads to high dissipation energy while a rigid, closely packed layer does not deform and as a result has low dissipation energy. rTp0483 adsorption on $-CH_3$ SAMs resulted in the lowest energy configuration, while adsorption on −OH SAMs resulted in the highest energy configuration. This indicates that on a hydrophobic surface rTp0483 forms a more tightly packed layer with low fluidity, and on a hydrophilic surface rTp0483 forms a much more deformable, fluid layer. The dissipation energy for rTp0483 on $-COO^-$ and $-NH_3^+$ SAMs was similar; however, there was a clear difference in both rTp0483 and FN adsorption. This difference can be explained as a combination of hydrophobic and charge effects. The observed trend is that the dissipation energy of rTp0483 is inversely proportional to hydrophobicity. By this logic, it would follow that rTp0483 adsorption on $-COO^-$ SAMs would result in a dissipation energy value close to that of an −OH SAM and slightly higher than an $-NH_3^+$ SAM, which in turn should be higher than a $-CH_3$ SAM. This, however, does not take into consideration the ionic properties of $-COO^-$ and $-NH_3^+$ SAMs. rTp0483 possesses a net positive charge under experimental conditions so it would be expected to bind more tightly to a negatively charged, hydrophilic surface than to a hydrophilic surface with no charge. By the same reasoning, binding to a positively charged surface would be looser than to an uncharged surface with similar hydrophobicity. It is also possible that this charge interaction contributes to the raised FN binding capacity of rTp0483 adsorbed onto $-COO^-$ SAMs. The observation that FN binds preferably to $-COO^-$ SAMs suggests that an interaction between the protein and the negative surface plays a role in FN binding. Specific areas of rTp0483 would be attracted to each of the functionalized SAM chemistries based on charge as well as hydrophobicity. It is possible that the binding orientation of rTp0483 differs based on surface chemistry, and that the FN binding site is only displayed when it is bound to $-COO^-$ SAMs. Another possibility is that the FN binding site of rTp0483 is normally concealed

within a fold of the protein, and when rTp0483 encounters a $-COO^-$ SAM a change in conformation occurs thereby exposing the binding site and allowing FN to bind.

FN binding with rTp0483 adsorbed on $-COO^-$ SAMs was analyzed at two rTp0483 concentrations in order to gain more information about the mechanism of binding. Initial analysis at 20 μg rTp0483/mL suggested a bivalent analyte mechanism as stated above. Since FN is a dimeric protein with two nearly identical units, each should be able to bind rTp0483, thus a bivalent analyte mechanism is reasonable. Assuming this convention, one unit of a FN molecule encounters and binds rTp0483 on the surface, followed by the second unit binding to an additional rTp0483 protein to complete the AB_2-type complex. Following this study, it was of interest to determine whether with decreasing rTp0483 surface mass density there existed a point where the distance between proteins became too great for adsorbed FN to reach the second rTp0483 required for AB_2 formation. For this purpose, the concentration of rTp0483 was reduced to 5 μg rTp0483/mL and FN adsorption was evaluated. Interestingly, the K_{A1} for FN adsorption was higher for 5 μg rTp0483/mL, while K_{A2} was higher for 20 μg rTp0483/mL. FN (440kDa) is significantly larger than rTp0483 (22kDa), so complete coverage of the surface by rTp0483 is not necessary and according to these results may actually lead to a lower surface mass density of FN. rTp0483 and FN adsorption studies along with AFM analysis suggest that protein aggregation on the surface may play a role. The most significant FN binding correlated to rTp0483 adsorbed on $-COO^-$ SAMs, which also displayed the smallest and most evenly distributed aggregate formation. As the rTp0483 concentration increases, the size of the protein aggregates would also likely increase. It is possible that as the aggregate size increases, the affinity for FN of proteins within the aggregate becomes limited due to steric hindrance. This agrees with the minimal FN binding to rTp0483 adsorbed on the other SAM surfaces, which displayed larger rTp0483 aggregates when compared to $-COO^-$ SAMs. Thus, at the lower concentration of 5 μg rTp0483/mL aggregates would be smaller, and likewise K_{A1} for FN greater. Conversely, at a concentration of 20 μg rTp0483/mL the size of rTp0483 aggregates would increase to limit the binding of a portion of rTp0483 proteins, leading to a smaller K_{A1}. The spacing of aggregates on each surface can help account for differences in K_{A2}. Once it has bound to rTp0483, FN would be stationary, and as a consequence, the chance of interacting with a second rTp0483 is limited to the range of motion of the unbound FN unit. While the initial affinity of FN for rTp0483 was less at 20 μg rTp0483/mL than at 5 μg rTp0483/mL, for the secondary binding event the distance between aggregates becomes important. At 20 μg rTp0483/mL the distance between aggregates is likely less than at 5 μg rTp0483/mL, and accordingly the chance that a bound FN is able to reach a second rTp0483 increases.

Unfortunately, the crystal structure of rTp0483 has not been elucidated; however, an estimation of its size can be made. The partial specific volume (υ) of a large number of globular proteins was determined experimentally to fall within a tight range from 0.70–0.75 cm^3/g.[38] Using this value as a starting point, an estimate of protein volume was made based on the rTp0483 molecular weight using equation 18. Here υ was assumed to fall in the middle of the range (0.73 cm^3/g), M_W (g/mol) was the molecular weight of rTp0483, and N_A was Avogadro's number (6.02×10^{23} molecules/mol).

$$\frac{\upsilon \times 10^{24}\frac{A^3}{cm^3} \times M_W}{N_A} \times 0.001\frac{nm^3}{A^3} = 1.21\times10^{-3} \times M_W \frac{nm^3}{molecule} \quad (18)$$

The molecular weight of rTp0483 is 22kDa, and the estimated volume is 27 nm^3. If surface adsorbed rTp0483 molecules are approximated as spheres the average surface area occupied

by a single rTp0483 molecule can be estimated. Based on this approximation the surface area occupied by an rTp0483 molecule is 11.3 nm^2.

The shape of rTp0483 likely varies from surface to surface based upon dissipation energy data; however, this is not as apparent in Figure 5 because the surfaces were dried prior to imaging, which may have impacted protein shape; however, based on Figure 5, it is apparent that for all surfaces the elevated areas have an area greater than 11.3 nm^2, which supports the theory that rTp0483 binds in aggregate form rather than as single proteins. The size of these protein islands was found to vary with surface chemistry. On $-NH_3^+$ SAMs, protein islands were larger compared to the other surfaces. For −OH and $-CH_3$ surfaces, rTp0483 islands were smaller than for $-NH_3^+$, while the distance between each island was similar. Adsorbed rTp0483 aggregates were the smallest on $-COO^-$ SAMs and were spread evenly across the entire surface. The size of the rTp0483 aggregates can be correlated to FN binding capacity. The $-COO^-$ SAMs displayed the least aggregation and the most uniform binding of rTp0483 across the surface. Because rTp0483 molecules are more spread out, it is probable that a greater number are able to take on an ideal binding configuration. As aggregates form, nearby rTp0483 may become restricted and thus access to potential binding sites could be inhibited.

Two peptide sequences of rTp0483 were identified as probable binding sites, and antibodies toward each were produced. The data show that anti-Tp0483#1 and anti-Tp0483#2 were able to inhibit FN binding to rTp0483 ($p<0.05$). When FN was added to rTp0483 prior to the antibodies, there was also a significant drop in antibody binding ($p<0.05$). Additionally, the two antibodies only bound to rTp0483 when immobilized on $-COO^-$ SAMs, which supports the idea that the targeted sites are obscured on all SAMs except for $-COO^-$.

Peptides matching the proposed FN binding sites on rTp0483 were synthesized and used to block FN. Peptides were evaluated because their small size eliminates the possibility of steric effects, which could result from blocking with the larger antibodies. Only D2 resulted in a significant decrease in FN binding ($p<0.05$). Based on this study, it appears that D1 did not play a direct role in FN-rTp0483 binding. It is probable that D2 plays some role; however, the observed reduction is not large enough to account for the entire binding event. The fact that significant inhibition was observed for both antibodies while little inhibition was seen for the specific peptides may indicate that the active FN binding sites of rTp0483 are located near the expressed sequences but do not coincide perfectly with them. Further characterization of the tertiary structure of Tp0483 is required to reach a conclusion.

FN domain studies were conducted to determine the regions of FN that are involved in rTp0483 binding. This was done based on changes in binding to FN when it was bound to rTp0483 compared to on unmodified $-COO^-$ SAMs. In a native environment, the RGD binding site of FN enables the protein to bind to cells and cellular components throughout the body, thereby modulating cell processes such as attachment, migration, growth, and differentiation.[14] It is also thought to play some role in the binding of FN by *T. pallidum*, which helps the bacteria to infiltrate the body via interactions with cells and the ECM.[1–3, 11–13] Further, it has been theorized that the adhesion of various host proteins, including FN, to the outer surface of *T. pallidum* partially contributes to the bacterium's ability to remain in the body for long periods of time between outbreaks. When FN was bound to rTp0483 adsorbed on $-COO^-$ SAMs, a 50% reduction in anti-RGD binding was observed compared to when FN was adsorbed on unmodified $-COO^-$ SAMs. To investigate further the involvement of the RGD site, an antibody specific to the cell-binding domain of FN was used to block the RGD peptide sequence in an effort to determine whether this site plays a role in rTp0483 binding. This study demonstrated a significant decrease in FN binding when blocked with 20 μg/mL anti-RGD, which agrees with previous reports that

indicated a measureable inhibition of *T. pallidum* binding to FN when it was incubated with anti-RGD.[12, 15–17]

The heparin-binding domains of FN were also examined as they have been implicated previously as potential bacterial targets on FN.[19] Results did not show strong heparin binding on either of the prepared protein coatings. One possible explanation lies in the location of the major heparin-binding sites. The stronger heparin II site is very close to the central cell-binding domain (CCBD), thus if there is an interaction in this region, it is reasonable to expect low binding on Tp0483+FN due to steric effects.[14] Low binding on FN can be accounted for based on electrostatic interactions. Heparin is strongly negative, and conversely, its binding site is strongly positive. When FN was adsorbed onto $-COO^-$ SAMs, the positively charged binding site could have been attracted to the negatively charged surface resulting in minimal binding. The balance of heparin binding can be accounted for by the weaker heparin I site; since it is located farther away from the cell-binding domain, it would remain unaffected by the binding of rTp0483 and FN.

Lastly, gelatin binding was examined. Gelatin is a denatured form of collagen; therefore, the gelatin-binding domain also serves as a binding domain for collagen. Like the CCBD and heparin-binding domains, certain species of bacteria have been shown to interact with FN through this domain.[18] Studies revealed an 80% reduction in gelatin binding when FN was bound to rTp0483 adsorbed on $-COO^-$ SAMs compared to FN bound to unmodified $-COO^-$ SAMs. This outcome suggests that the gelatin/collagen-binding domain of FN may play a role in rTp0483 binding.

CONCLUSIONS

Binding of *T. pallidum* recombinant protein fragment rTp0483 was shown to be greatest on negatively charged $-COO^-$ SAMs, while FN only bound in significant quantities to rTp0483 adsorbed on these surfaces. Kinetic analysis of rTp0483 adsorption revealed that the strength of the bond between the protein and each surface was dependent on the surface chemistry. Also, kinetic analysis of FN binding on adsorbed rTp0483 demonstrated that the surface mass density of rTp0483 affects the strength of FN binding. Decreasing the concentration of adsorbed rTp0483 from 20 to 5 μg/mL increased K_{A1} and decreased K_{A2} for FN binding. A blocking study toward the RGD sequence of FN demonstrated an involvement in rTp0483 binding, and through the use of antibodies and peptides, rTp0483 amino acids 316–333 were observed to play a role in FN binding. A QCM study examining the dissipation energy to frequency shift ratio of rTp0483 adsorption to functionalized SAMs suggested different binding configurations based on surface chemistry, while AFM analysis illustrated that rTp0483 binds as protein aggregates rather than single proteins. FN binding domain studies reinforced the importance of the RGD sequence and pointed toward the association of the collagen/gelatin-binding domain in rTp0483 binding. Through the development of an rTp0483 surface coating capable of binding FN with high affinity it will be possible to analyze the effect of rTp0483 on various aspects of the host response with and without FN in a manner resembling natural Tp0483 on the surface of *T. pallidum*. In the future this may lead to a better understanding of *T. pallidum* as well as potential applications in development of materials with antigenic disguise properties.

Supplementary Material

Refer to Web version on PubMed Central for supplementary material.

Acknowledgments

We would like to thank Dr. Tonglei Li for the use of his contact angle goniometer, Jeffrey Lenihan for his protein purification contributions, and the Institute of Advanced Materials and Renewable Energy at the University of Louisville for the use of its XPS facility. This work was supported by an NSF Integrative Graduate Education and Research Traineeship (IGERT) program on Engineered Bioactive Interfaces and Devices at the University of Kentucky (DGE-0653710), by NASA (KWA and MBA), and by the Public Health Service grant AI-51334 (CEC) from the National Institutes of Health.

REFERENCES

1. Brinkman MB, McGill MA, J P, Rogers A, Matejkova P, Smajs D, Weinstock GM, Norris SJ, Palzkill T. A novel Treponema pallidum antigen, Tp0136, is an outer membrane protein that binds human fibronectin. Infection and Immunity. 2008; 76:1848–1857. [PubMed: 18332212]
2. Cameron CE. Identification of a *Treponema pallidum* Laminin-Binding Protein. Infection and Immunity. 2003; 71:2525–2533. [PubMed: 12704124]
3. Cameron CE, Brown EL, Kuroiwa JMY, Schnapp LM, Brouwer NL. *Treponema pallidum* fibronectin-binding proteins. Journal of Bacteriology. 2004; 186:7019–7022. [PubMed: 15466055]
4. Cox DL, Luthra A, Dunham-Ems S, Desrosiers DC, Salazar JC, Caimano MJ, Radolf JD. Surface immunolabeling and consensus computational framework to identify candidate rare outer membrane proteins of *Treponema pallidum*. Infection and Immunity. 2010; 78:5178–5194. [PubMed: 20876295]
5. Desrosiers DC, Anard A, Luthra A, Dunham-Ems SM, LeDoyt M, Cummings MAD, Eshghi A, Cameron CE, Cruz AR, Salazar JC, Caimano MJ, Radolf JD. Tp0326, a Treponema pallidum β-barrel assembly machinery A (BamA) orthologue and rare outer membrane protein. Molecular Microbiology. 2011; 80:1496–1515. [PubMed: 21488980]
6. Liu SQ, Wang SP, Wu YM, Zhao FJ, Zeng TB, J ZY, Zhang QG, Gao DM. Production of proinflammatory cytokines in the human THP-1 monocyte cell line following induction by Tp0751, a recombinant protein of *Treponema pallidum*. Science China, Life Sciences. 2010; 53:229–233. [PubMed: 20596832]
7. Radolf JD. Role of outer membrane architecture in immune evasion by *Treponema pallidum* and *Borrelia burgdorferi*. Trends in Microbiology. 1994; 2:307–311. [PubMed: 7812663]
8. Salazar JC, Hazlett KRO, Radolf JD. The immune response to infection with *Treponema pallidum* the stealth pathogen. Microbes and Infection. 2002; 4:1133–1140. [PubMed: 12361913]
9. Tomson FL, Conley PG, Norgard MV, Hagman KE. Assessment of cell-surface exposure and vaccinogenic potentials of *Treponema pallidum* candidate outer membrane proteins. Microbes and Infection. 2007; 9:1267–1275. [PubMed: 17890130]
10. Anderson KV. Toll signalling pathways in the innate immune response. Current Opinion in Immunology. 2000; 12:13–19. [PubMed: 10679407]
11. Fitzgerald TJ, Repesh LA. Interaction of fibronectin with *Treponema pallidum*. Genitourinary Medicine. 1985; 61:147–155. [PubMed: 3891582]
12. Lee JH, Choi HJ, Jung J, Lee MG, Lee JB, Lee KH. Receptors for *Treponema pallidum* attachment to the surface and matrix proteins of cultured human dermal microvascular endothelial cells. Yonsei Medical Journal. 2003; 44:371–378. [PubMed: 12833573]
13. Peterson KM, Baseman JB, Alderete JF. *Treponema pallidum* receptor binding proteins interact with fibronectin. Journal of Experimental Medicine. 1983; 157:1958–1970. [PubMed: 6304227]
14. Pankov R, Yamada KM. Fibronectin at a glance. Journal of Cell Science. 2002; 115:3861–3863. [PubMed: 12244123]
15. Ouaissi MA. Role of the RGD sequence in parasite adhesion to host cells. Parasitology Today. 1988; 4:169–173. [PubMed: 15463077]
16. Thomas DD, Baseman JB, Alderete JF. Fibronectin mediates Treponema pallidum cytadherence through recognition of fibronectin cell-binding domain. Journal of Experimental Medicine. 1985; 161:514–525. [PubMed: 3156205]
17. Thomas DD, Baseman JB, Alderete JF. Fibronectin tetrapeptide is target for syphilis spirochete cytoadherence. Journal of Experimental Medicine. 1985; 162:1715–1719. [PubMed: 3903025]

18. Atkin KE, Brentnall AS, Harris G, Bingham RJ, Erat MC, Millard CJ, Schwarz-Linek U, Staunton D, Vakonakis I, Campbell ID, Potts JR. The streptococcal binding site in the gelatin-binding domain of fibronectin is consistent with a non-linear arrangement of modules. The Journal of Biological Chemistry. 2010; 285:36977–36983. [PubMed: 20843804]
19. van der Flier M, Chhun N, Wizemann TM, Min J, McCarthy JB, Tuomanen EI. Adherence of *Streptococcus pneumoniae* to immobilized fibronectin. Infection and Immunity. 1995; 63:4317–4322. [PubMed: 7591065]
20. Cameron CE, Lukehart SA, Castro C, Molini B, Godornes C, Van Voorhis WC. Opsonic potential, protective capacity, and sequence conservation of the Treponema pallidum subspecies pallidum Tp92. The Journal of Infectious Disease. 2000; 181:1401–1413.
21. Zhang HH, Blanco DR, Exner MM, Shang ES, Champion CI, Phillips ML, Miller JN, Lovett MA. Renaturation of recombinant *Treponema pallidum* rare outer membrane protein 1 into a trimeric, hydrophobic, and porin-active conformation. Journal of Bacteriology. 1999; 181:7168–7175. [PubMed: 10572117]
22. Chung YC, Chiu YH, Wu YW, Tao YT. Self-assembled biomimetic monolayers using phospholipid-containing disulfides. Biomaterials. 2005; 26:2313–2324. [PubMed: 15585234]
23. Keselowsky BG, Collard DM, Garcia AJ. Surface chemistry modulates fibronectin conformation and directs integrin binding and specificity to control cell adhesion. Journal of Biomedical Materials Research Part A. 2003; 66A:247–259. [PubMed: 12888994]
24. Ling JC, Chuang WH. Synthesis, surface characterization, and platelet reactivity evaluation for the self-assembled monolayer of alkanethiol with sulfonic acid functionality. Journal of Biomedical Materials Research. 2000; 51:413–423. [PubMed: 10880084]
25. Michael KE, Vernekar VN, Keslowsky BG, Meredith JC, Latour RA, Garcia AJ. Adsorption-induced conformational changes in fibronectin due to interactions with well-defined surface chemistries. Langmuir. 2003; 19:8033–8040.
26. Nuzzo RG, Dubois LH, Allara DL. Fundamental studies of microscopic wetting on organic surfaces. 1. Formation and structural characerization of self-consistent series of polyfunctional organic monolayers. Journal of the American Chemical Society. 1990; 112:558–569.
27. Sperling C, Schweiss RB, Streller U, Werner C. *In vitro* hemocompatibility of self-assembled monolayers displaying various functional groups. Biomaterials. 2005; 26:6547–6557. [PubMed: 15939466]
28. Tanahashi M, Matsuda T. Surface functional group dependence on apatite formation on self-assembled monolayers in a simulated body fluid. Journal of Biomedical Materials Research. 1997; 34:305–315. [PubMed: 9086400]
29. Dixon MC. Quartz crystal microbalance with dissipation monitoring: Enabling real-time characterization of biological materials and their interactions. Journal of Biomolecular Techniques. 2008; 19:151–158. [PubMed: 19137101]
30. Hemmersam AG, Rechendorff K, Foss M, Sutherland DS, Besenbacher F. Fibronectin adsorption on gold, Ti-, and Ta-oxide investigated by QCM-D and RSA modelling. Journal of Colloid and Interface Science. 2008; 320:110–116. [PubMed: 18201712]
31. Stenberg E, Persson BRH, Urbaniczky C. Quantitative determination of surface concentration of protein with surface plasmon resonance by using radiolabeled proteins. Colloids and Interface Science. 1991; 143:513–526.
32. BIAevaluation 3.0 Software Handbook. Uppsala, Sweden: Biacore AB; 1997.
33. Benesch J, Svedhem S, Svensson SCT, Valiokas R, Liedberg B, Tengvall P. Protein adsorption to oligo(ethylene glycol) self-assembled monolayers: Experiments with fibrinogen, heparinized plasma, and serum. Journal of Biomaterials Science, Polymer Edition. 2001; 12:581–597. [PubMed: 11556738]
34. Fischer M, Sperling C, Werner C. Synergistic effect of hydrophobic and anionic surface groups triggers blood coagulation *in vitro*. Journal of Materials Science: Materials in Medicine. 2010; 21:931–937. [PubMed: 19851837]
35. Lestelius M, Liedberg B, Tengvall P. *In vitro* plasma protein adsorption on w-functionalized alkanethiolate self-assembled monolayers. Langmuir. 1997; 13:5900–5908.

36. Rodrigues SN, Goncalves IC, Martins MCL, Barbosa MA, Ratner BD. Fibrinogen adsorption, platelet adhesion and activation on mixed hydroxyl-/methyl-terminated self-assembled monolayers. Biomaterials. 2006; 27:5357–5367. [PubMed: 16842847]

37. Sperling C, Fischer M, Maitz MF, Werner C. Blood coagulation on biomaterials requires the combination of distinct activation processes. Biomaterials. 2009; 30:4447–4456. [PubMed: 19535136]

38. Harpaz Y, Gerstein M, Chothia C. Volume changes on protein folding. Structure. 1994; 15:641–649. [PubMed: 7922041]

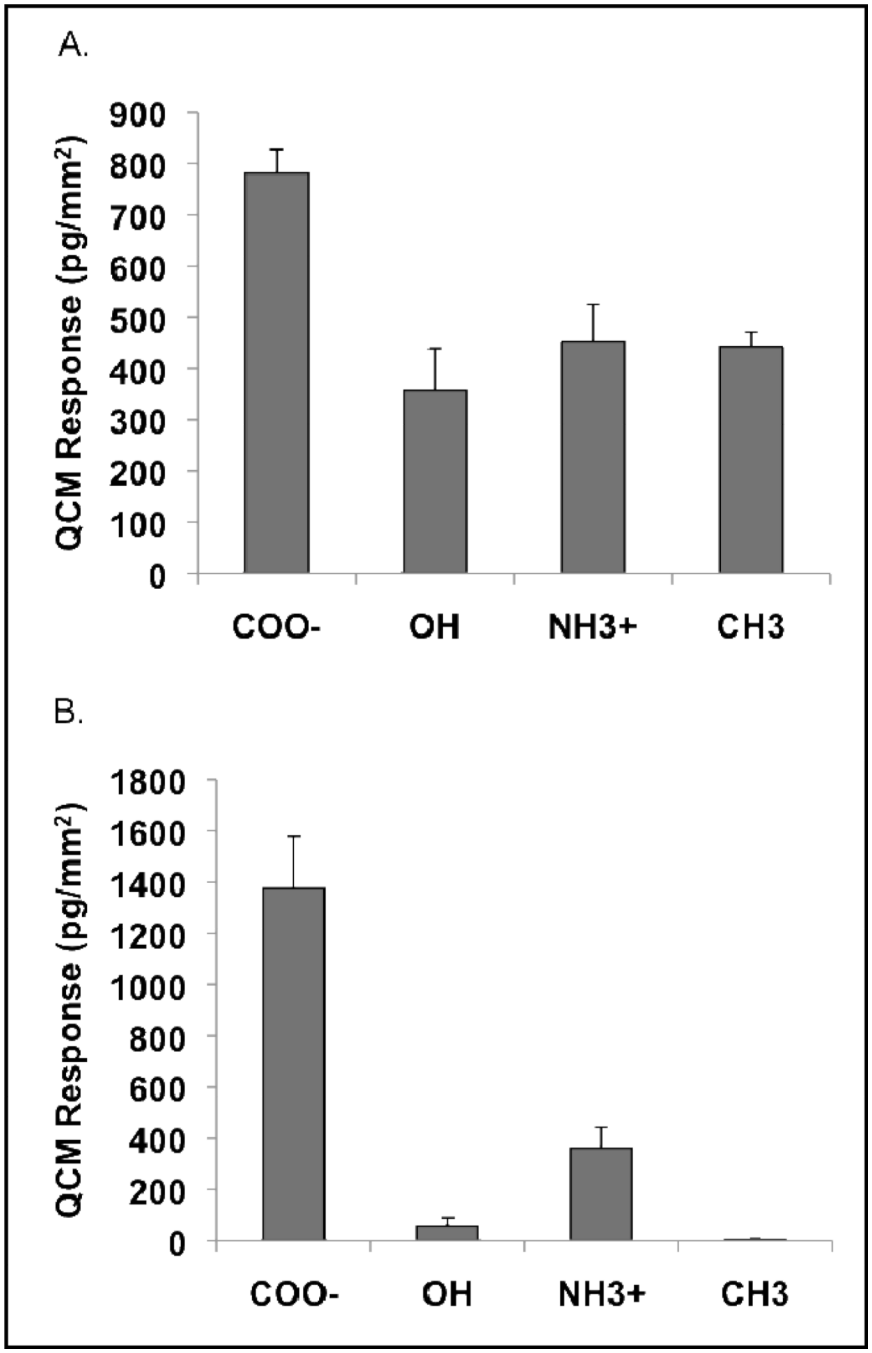

Figure 1.

(A) Average rTp0483 binding on SAMs determined by QCM and (B) average FN binding to adsorbed rTp0483 on SAMs determined by QCM. ANOVA indicates higher rTp0483 and FN binding on $-COO^-$ SAMs ($p<0.05$). Data is reported as a mean (n=3) for all sample groups with error bars representing standard error.

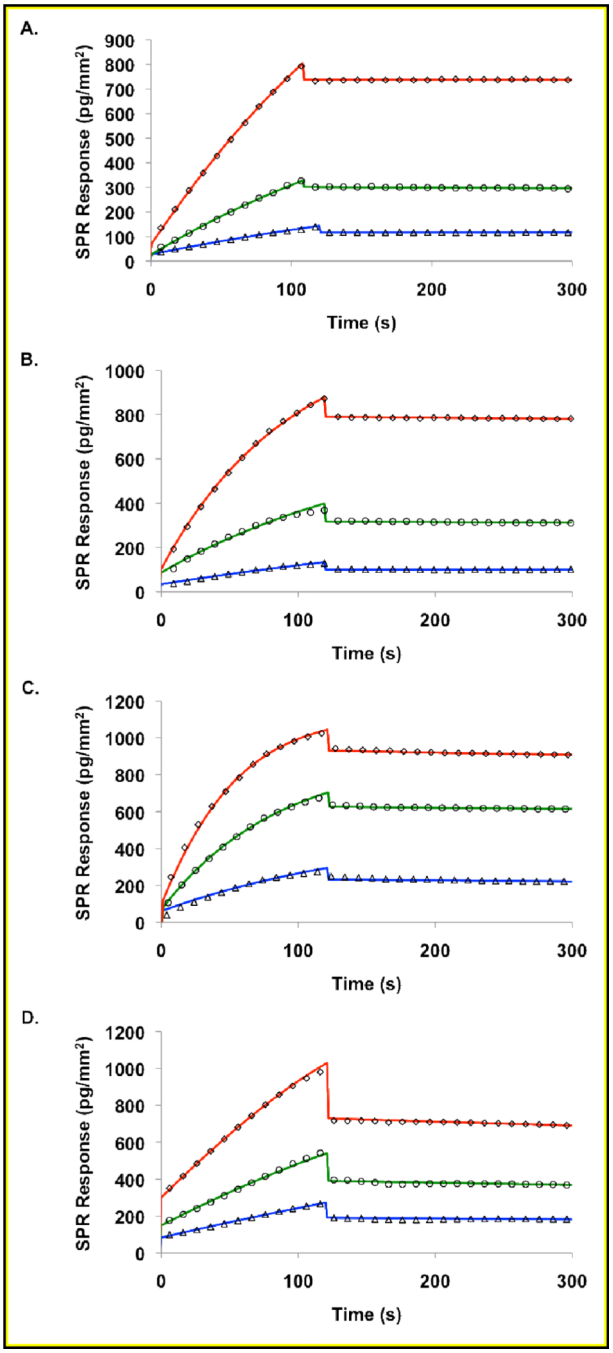

Figure 2.

1:1 Langmuir binding with mass transport limitations for rTp0483 adsorption onto SAMs at 5 (Δ), 10 (○), and 20 (◊) μg rTp0483/mL with surfaces functionalized with (A) $-COO^-$, (B) $-OH$, (C) $-CH_3$, and (D) $-NH_3^+$. Solid lines are predicted fits based on 1:1 Langmuir binding with mass transport limitations for 5 (—), 10 (—), and 20 (—) μg rTp0483/mL.

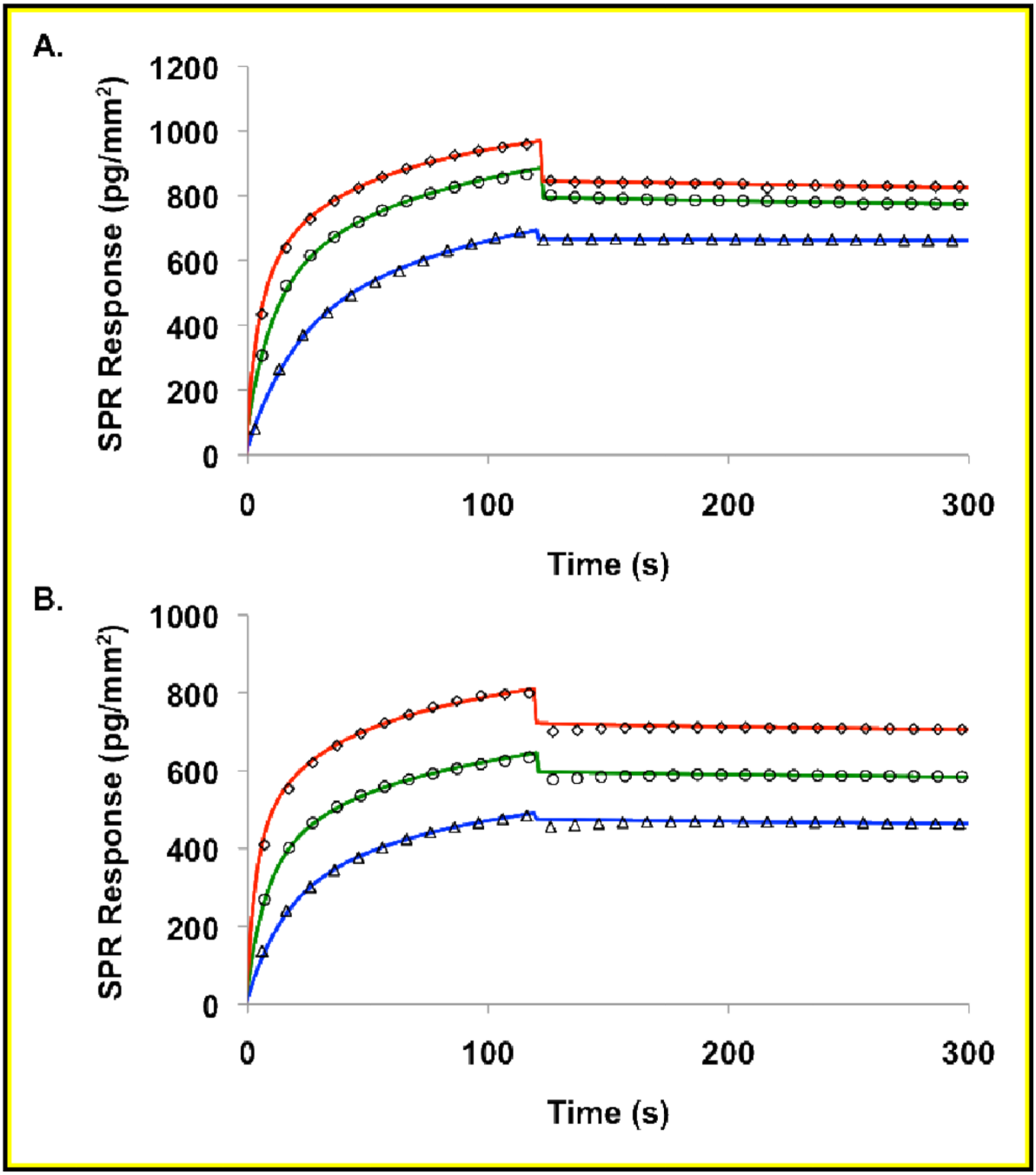

Figure 3.

Bivalent FN binding to adsorbed rTp0483 on −COO^- SAMs at 10 (Δ), 20 (○), and 40 (◊) μg FN/mL with (A) 5 μg rTp0483/mL and (B) 20 μg rTp0483/mL rTp0483 adsorbed. Solid lines are predicted fits based on a bivalent analyte model for 10 (—), 20 (—), and 40 (—) μg FN/mL.

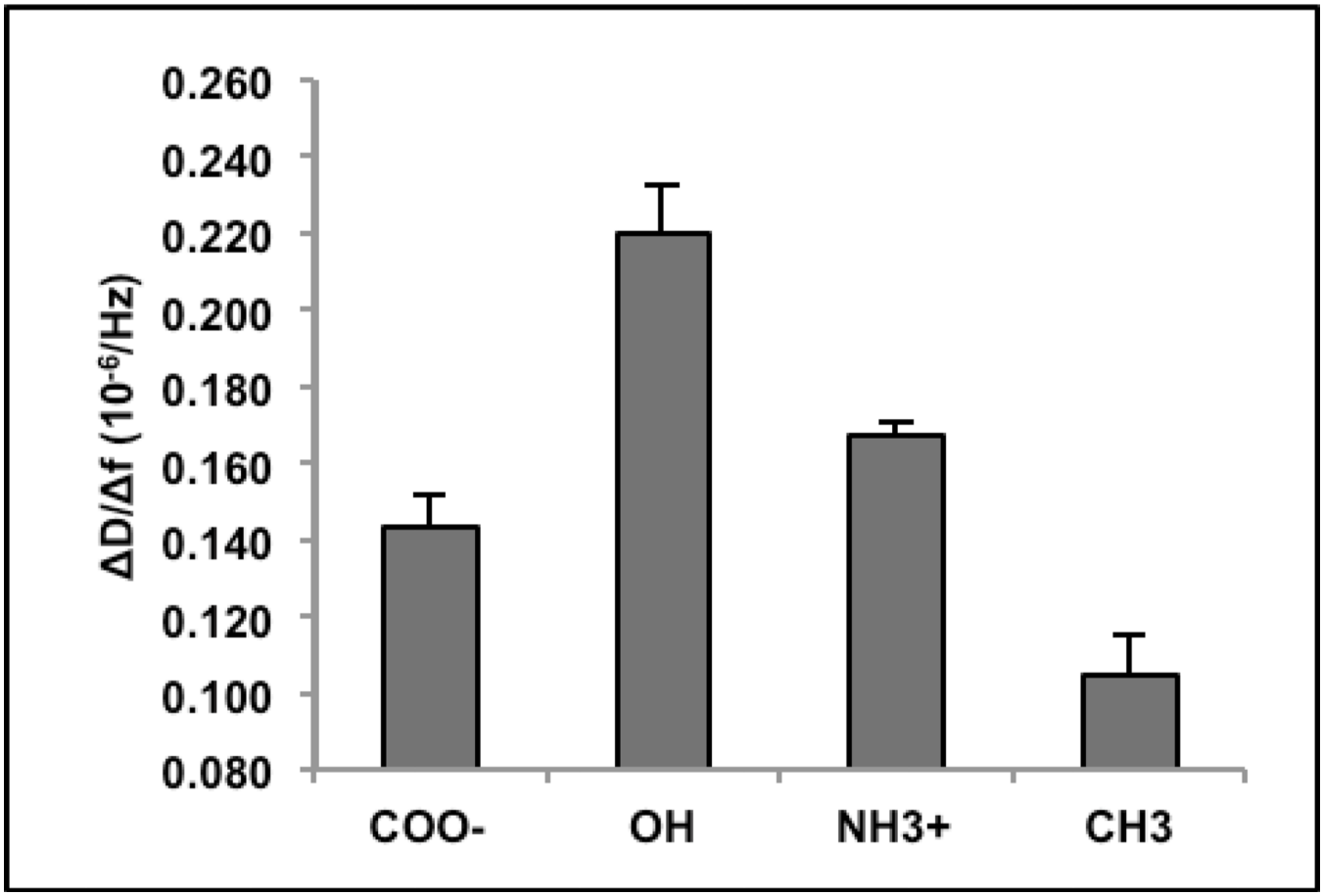

Figure 4.

Ratio of QCM dissipation energy change (ΔD) to frequency shift (Δf) for rTp0483 adsorption at 100 μg rTp0483/mL on functionalized SAMs. ANOVA indicates a difference between the groups with −OH being the highest, $-CH_3$ being the lowest, and $-COO^-$ and $-NH_3^+$ being statistically indistinguishable. Data are reported as a mean (n=3) for all sample groups with error bars representing standard error.

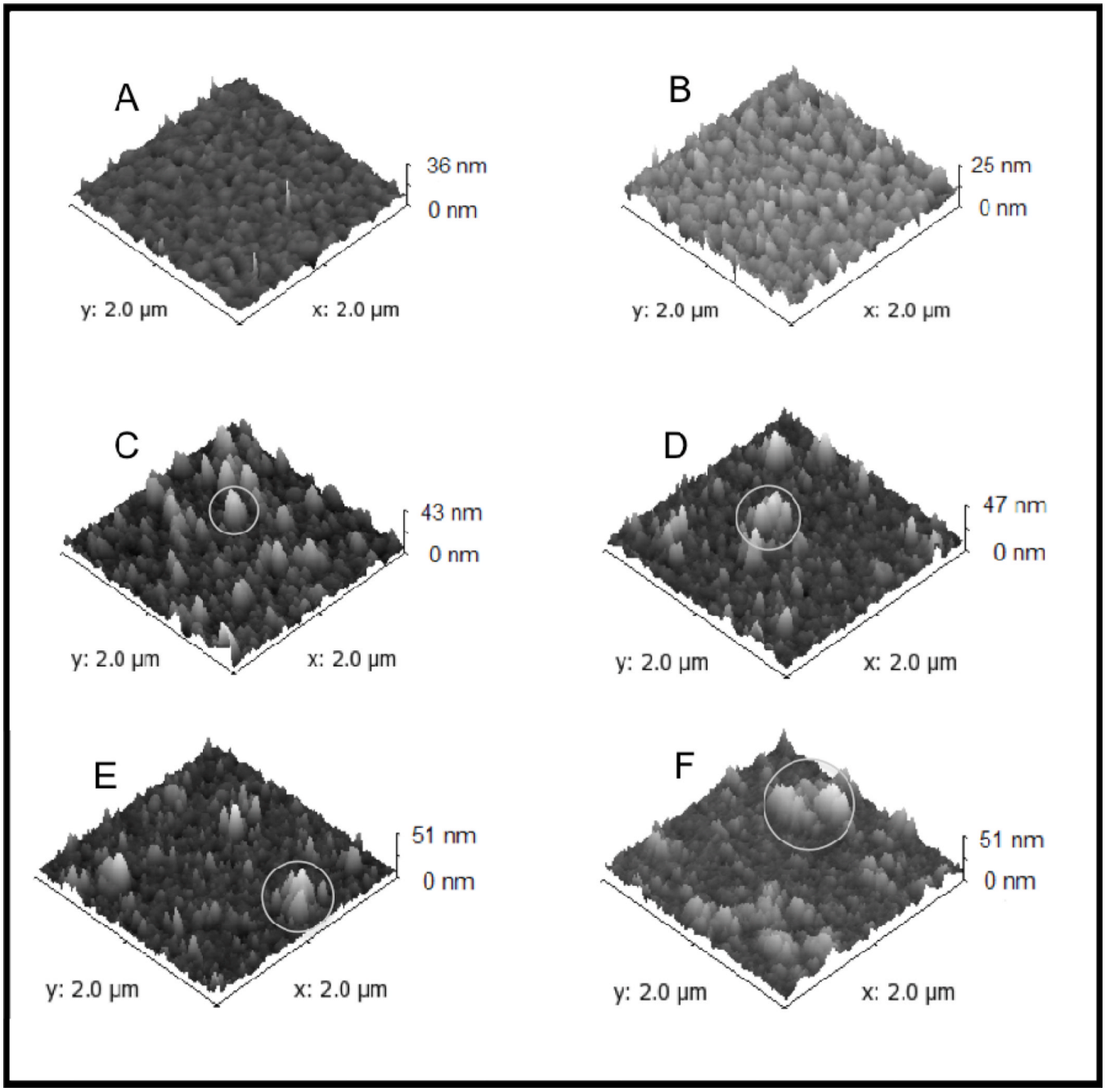

Figure 5.

AFM comparison of gold, a model $-CH_3$ SAM and 10 µg rTp0483/mL coated SAMs. (A) Unmodified gold surface, (B) model SAM ($-CH_3$), (C) rTp0483 on $-COO^-$ SAM, (D) rTp0483 on $-CH_3$ SAM, (E) rTp0483 on −OH SAM, and (F) rTp0483 on $-NH_3^+$ SAM. Representative areas with aggregated proteins are noted.

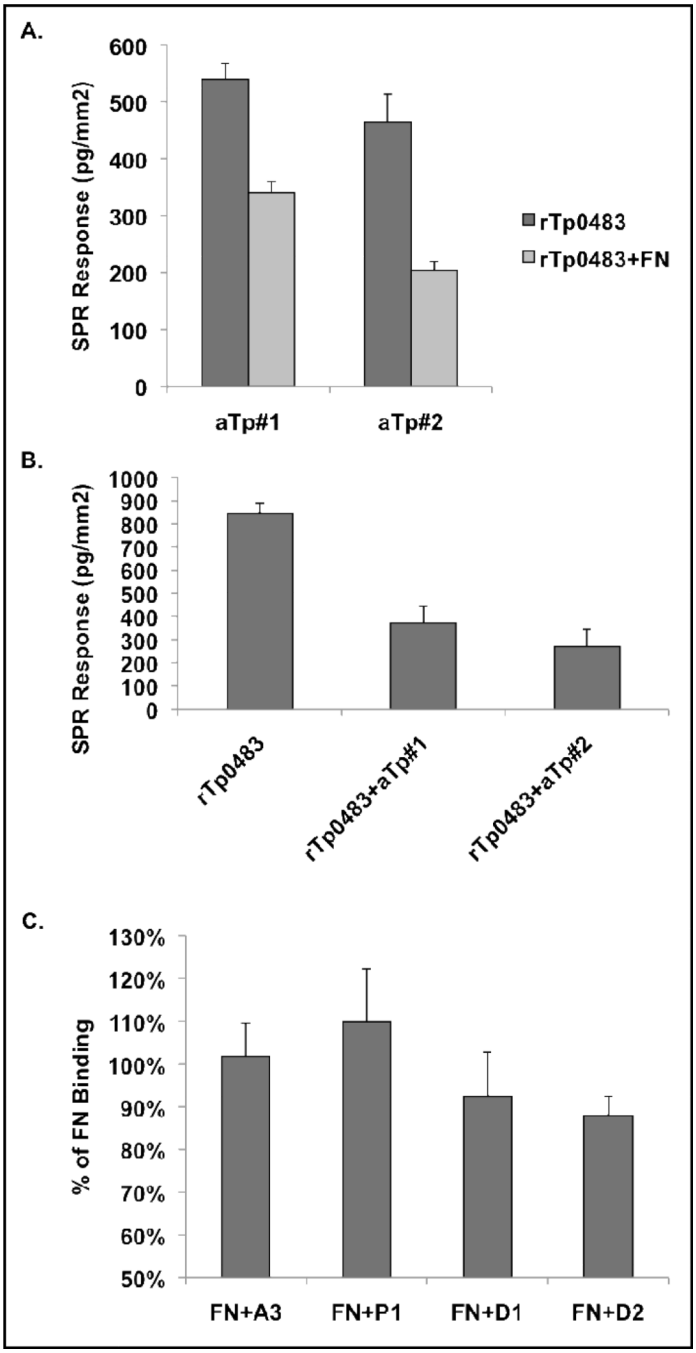

Figure 6.

rTp0483 binding site studies. (A) anti-rTp0483 antibody binding on surfaces with adsorbed rTp0483 or rTp0483+FN, (B) FN binding on surfaces with adsorbed rTp0483 with and without antibodies, (C) FN binding when blocked with peptide sequences compared to FN alone on surfaces with adsorbed rTp0483. Binding of FN to rTp0483 reduced the binding of aTp#1 and aTp#2 ($p<0.05$). Data represent mean (n=2) with error bars representing standard error. Binding of FN onto rTp0483 and aTp#1 or aTp#2 was lower than binding of FN on rTp0483 alone ($p<0.05$). Data represent mean (n=2) with error bars representing standard error. Peptide D2 reduced FN binding ($p<0.05$). Data represent mean (n=6) with error bars representing standard error.

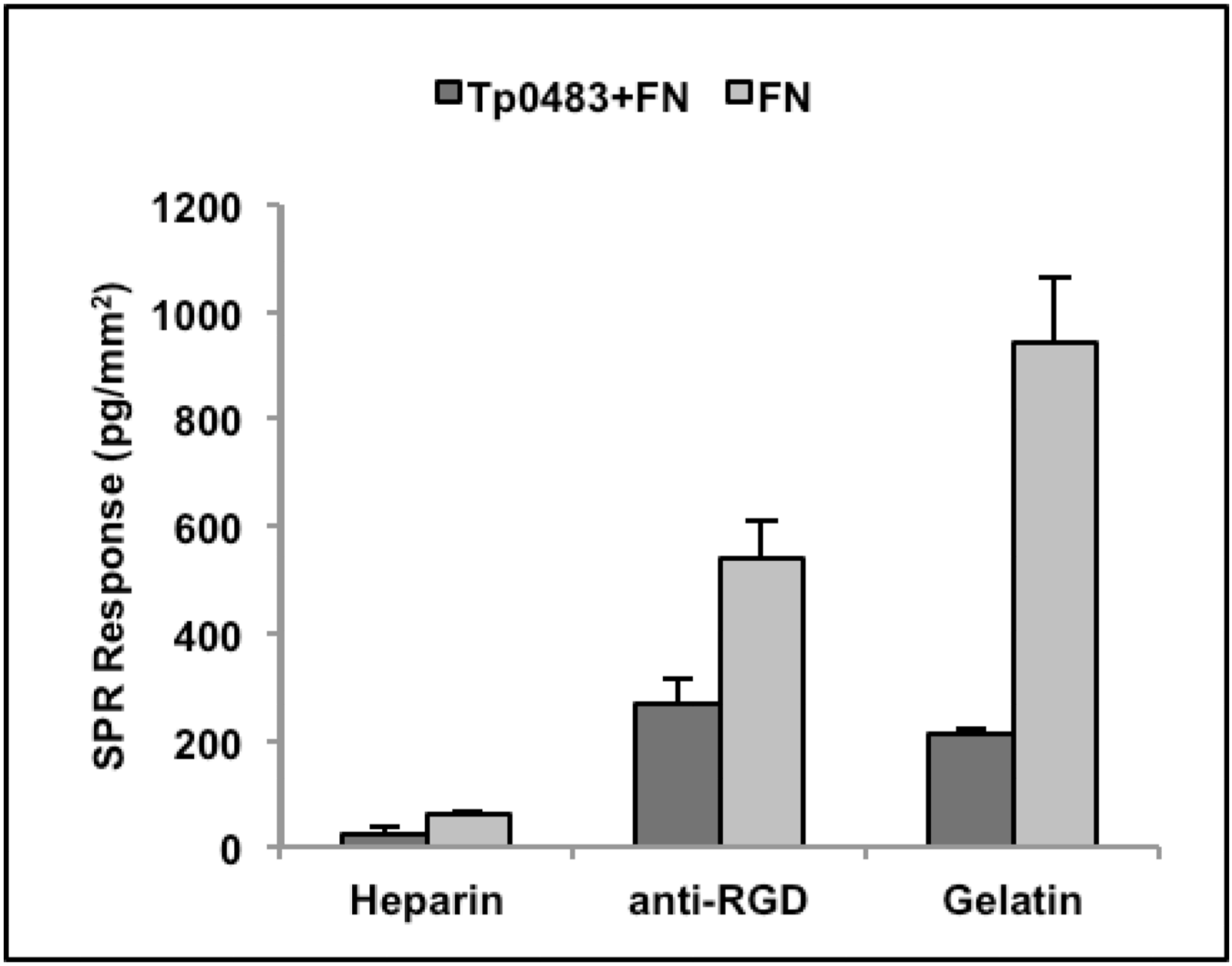

Figure 7.

Binding of heparin, anti-RGD antibody, and gelatin to FN or rTp0483+FN on $-COO^-$ SAMs. Binding to Tp0483+FN was determined to be significantly less than to FN for anti-RGD and gelatin ($p<0.05$). Data represent mean (n=3) with error bars representing standard error.

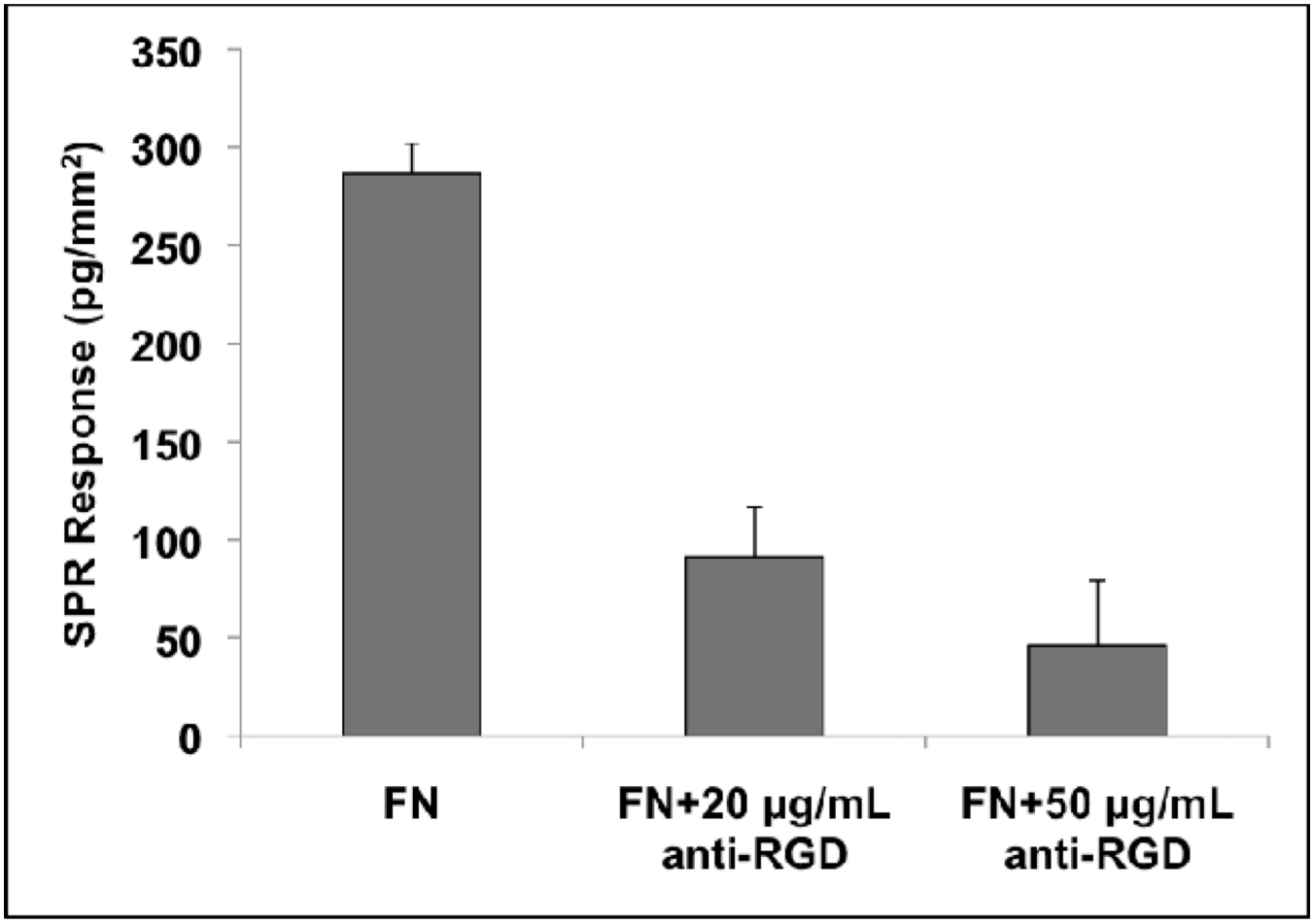

Figure 8.
Comparison of the binding of FN to rTp0483 versus the binding of FN when blocked with 20 or 50 µg/mL anti-RGD. Significant inhibition was observed at a concentration of 20 µg/mL anti-RGD ($p<0.05$). No statistical difference was noted between 20 µg/mL and 50 µg/mL anti-RGD. Data are reported as a mean with error bars representing standard error (n=10 for FN, n=5 for 20 µg/mL anti-RGD, and n=5 for 50 µg/mL anti-RGD).

Table 1

Kinetic constants for 1:1 Langmuir binding with mass transport limitations for rTp0483 binding on functionalized SAMs. [c]

SAM type	K_A (1/M) [a]	chi^2 (RU) [b]
$-COO^-$	$(13.10\pm0.19)\times10^7$	2.5
$-OH$	$(7.23\pm0.21)\times10^7$	2.4
$-CH_3$	$(4.93\pm0.08)\times10^7$	3.7
$-NH_3^+$	$(5.12\pm0.25)\times10^7$	4.7

(a) K_A- affinity constant;

(b) Chi^2- goodness of fit;

(c) K_A was significantly different between surfaces ($p<0.05$) except for $-CH_3$ and NH_3^+, which were the same (n=3).

Table 2

Kinetic constants for bivalent FN binding to rTp0483 on $-COO^-$ SAMs. [c]

rTp0483 (μg/mL)	K_{A1} (1/M) [a]	K_{A2} (1/RU) [b]	Chi^2 (RU)
5	$(1.53\pm0.13) \times 10^9$	$(2.25\pm0.21) \times 10^2$	4.8
20	$(1.03\pm0.08) \times 10^9$	$(4.03\pm0.47) \times 10^2$	4.0

(a) K_{A1}- affinity constant for reaction 1;

(b) K_{A2}- affinity constant for reaction 2;

(c) K_{A1} and K_{A2} were significantly different between 5 and 20 μg/mL adsorbed rTp0483 ($p<0.05$) (n=3).